MICROSTRUCTURAL ANALYSIS OF CANCELLOUS BONE TAKING INTO ACCOUNT GEOMETRICALLY NON-LINEAR EFFECTS

Olga Roa[†], Carlos M. López[††], Paola Pisoni[†††], Monica Pini[†††], Ignacio Carol[†],

Roberto Contro[†††]

[†]ETSECCPB (School of Civil Engineering), UCP (Technical Univ. of Catalunya)
Jordi Girona 1-3, E-08034 Barcelona, Spain
e-mail: Olga.Roa@upc.es, Ignacio.Carol@upc.es
[††]ICMAB (CSIC Institute of Material Science, Barcelona)
Campus UAB, E-08193 Bellaterra, Spain
e-mail: Carlos.Maria.Lopez@upc.es
[†††]Dept. of Structural Engineering, Politecnico di Milano
Piazza Leonardo da Vinci 32, I-20133 Milano, Italy
e-mail: contro@stru.polimi.it

Key words: Trabecular Bone, Microstructural Analysis, Interface Constitutive Model, Finite Element Analysis, Large Displacements.

Abstract. The mechanical behavior of trabecular bone specimens in tension and compression is studied numerically via microstructural simulation. Numerically generated microstructural geometries are used, which has similar statistical parameters as the ones calculated from digitalized images of real bone samples. In the FE calculations, material behavior for the continuum elements is assumed linear elastic and the possibility of cracking is introduced by inserting interface elements along most relevant potential crack paths. Interface behavior is given by a fracture energy-based work-softening plastic model with a coupled normal-shear hyperbolic failure surface. Although strains in the continuum and relative displacements at the interfaces are assumed small, large displacement capability is introduced in the FE analysis, in order to capture buckling of cell walls and change of orientation of material bridges which may have significant influence on the peak compressive strength and residual tensile behavior, respectively. Calculations with and without geometric non-linear effects are performed, and the results are compared and discussed with experimental data from the literature.

1

1 INTRODUCTION

Cancellous bone tissue is an inhomogeneous porous structure. The cancellous structure is a lattice of narrow rods and plates of calcified tissue called trabeculae, surrounded by vascular marrow which provides nutrients and waste disposal for the bone cells (Figure 1). Due to a progressive increase in the use of implanted bone devices, a clinical need is developing to understand the mechanical and remodeling behaviour of bone tissue[1,2,3]. Detailed understanding of complex aspects of fracture of heterogeneous materials may be improved with explicit consideration of their microstructure. Some studies of this kind, using the FEM, can be found in literature on concrete[4,5,6] and cancellous bone[7,8,9].
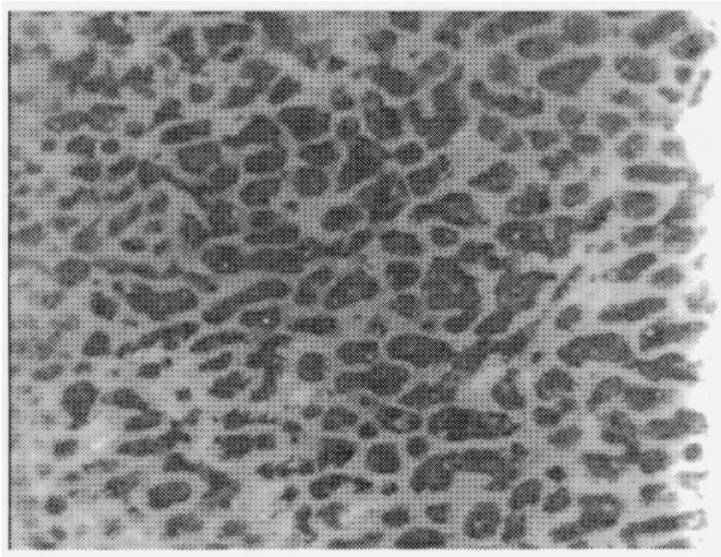
Figure 1. Side view of a trabecular bone specimen.

In this paper, on-going numerical research along this line, being carried out at ETSECCPB-UPC in cooperation with Politecnico di Milano, is summarized. Preliminar studies showed that microstructural models incorporating fracture-based interface elements similar to the ones used for concrete, could be applied successfully to obtain the peak load and failure patterns of the tensile behavior of cancellous bone[10]. Current efforts aim at incorporating non-linear geometric effects in the FE analysis, in order to be able to capture the micro-buckling of trabeculae in compression, and also to eliminate unrealistic residual stresses at large tensile strains.

2 MICROSTRUCTURAL DISCRETIZATION AND MESHES

In the work presented, the computer analyses have been run on meshes generated numerically according to the average geometric characteristics measured in real bone. A mesh of regular hexagons has been defined as a function of some stochastic parameters, such as the

number of hexagons in the two directions *x* and *y*, and the semi-length of the hexagon edge. Subsequently, a distortion and shrinking of the mesh is applied to reproduce the distribution and density of pores within the matrix. The trabecular matrix is discretized with triangular finite elements with linear elastic behavior. The FE model mesh includes a number of zero-thickness interface elements in between the continuum triangles. The constitutive behavior of the interfaces is described in the following section. A 10 x 10 mm specimen is represented in 2-D by two alternative arrangements which differ in the discretization of the specimen boundary: in one case the specimen boundary goes through the matrix, in the other the boundary crosses voids. Figure 2 shows the two meshes with all the continuum elements (left) and with only interface elements (right). The interface elements have been included along selected boundaries to provide non-tortuous failure paths. Mesh 1 contains 1360 triangles, 1061 interface elements and 2736 nodes, while mesh 2 has 1336 triangles, 974 interface elements and 2500 nodes.
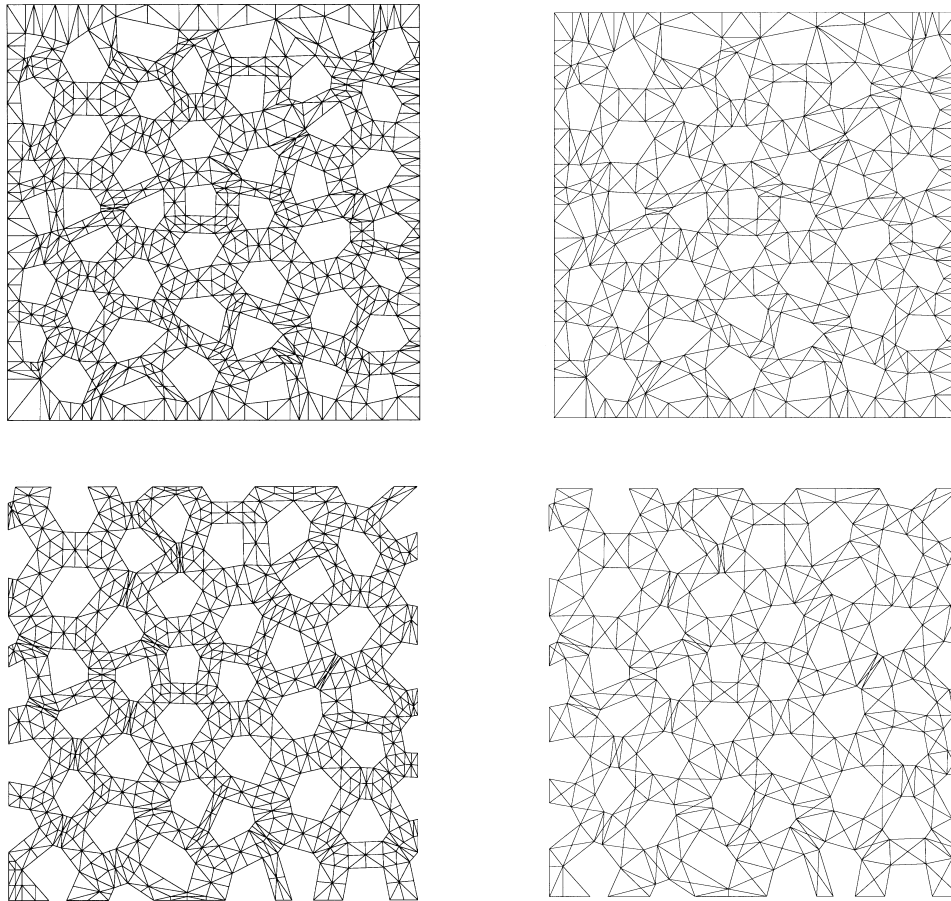
Figure 2. FE discretization of trabecular architecture for mesh 1 (up) and mesh 2 (down) with all continuous elements (left) and with only interface elements (right).

3 INTERFACE CONSTITUTIVE MODEL

Interface behavior is formulated in terms of the normal and shear components of stresses (tractions), $\boldsymbol{\sigma} = [\sigma_N, \ \sigma_T]^t$, and corresponding relative displacements $\mathbf{u} = [u_N, \ u_T]^t$ (^{t}=transposed). The model has been used for individual discrete cracks[11] and for each potential crack plane in a continuum-type multicrack model[12]. It conforms to work-softening elasto-plasticity, where plastic relative displacements can be identified with crack openings. The main features of the plastic model are represented in Figure 3. The initial loading (failure) surface $F = 0$ is a three-parameter hyperbola (tensile strength χ, c and $\tan\phi$; Figure 3a). The model is associated in tension ($Q = F$), but not in compression, where dilatancy vanishes progressively for $\sigma_N \to \sigma^{dil}$. Classic Mode I fracture occurs in pure tension. A second Mode IIa is defined under shear and high compression, with no dilatancy (Figure 3b). The fracture energies G^I_f and G^{IIa}_f are two model parameters. After initial cracking, c and χ decrease (Figure 3d), and the loading surface shrinks, degenerating in the limit case into a pair of straight lines representing pure friction (Figure 3c). The process is driven by the energy spent in fracture process, W^{cr} = plastic work, less frictional work in compression. Total exhaustion of tensile strength ($\chi = 0$) is reached for $W^{cr} = G^I_f$, and residual friction ($c = 0$) is reached for $W^{cr} = G^{IIa}_f$. Additional parameters α_χ and α_c allow for different shapes of the softening laws (linear decay for $\alpha_\chi = \alpha_c = 0$). The elastic stiffness matrix is diagonal with K_N, K_T, that can be regarded simply as penalty coefficients. More details can be found in[11].
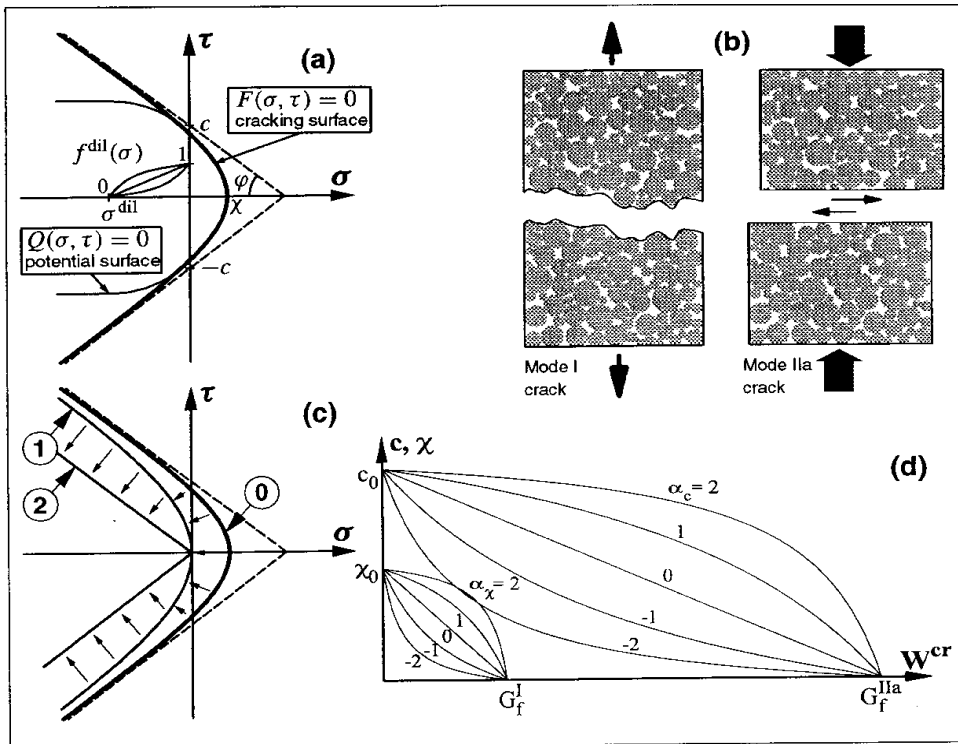
Figure 3. Interface model: (a) failure surface and plastic potential, (b) basic modes of fracture, (c) softening laws, and (d) evolution of the failure surface.

4 GEOMETRIC NONLINEAR EFFECTS

Non-negligeable geometric nonlinear effects associated to large displacements and rotations may take place in compression due to the relative slenderness of the trabeculae, and in tension due to the remaining bridges of material at advanced stages of the decohesive process.

In the assumption that the strains of the continuum elements and the relative displacements of the interfaces remain small, these nonlinear effects are introduced by means of an *Incremental Lagrangian* formulation of the FE method. This approximate procedure requires small steps, but small steps have to be taken anyway in this type of analysis due to the highly nonlinear character of the interface softening laws and the overall resulting material behavior.

Since strains remain small, there will be only two types of relevant strain and stress measures at a point of the structure. The Lagrangian or *material* strains and stresses, denoted as $\mathring{a}_{mat}$, $\acute{o}_{mat}$, would be those measured by an observer sitted on that point of the structure and moving with it, and are those which should enter the constitutive equations. The Eulerian or *spatial* stress and strain, denoted $\mathring{a}_{spa}$, $\acute{o}_{spa}$, would be those measured by an observer looking at the structure from an outside fixed position on the axes *x, y*.

Using standard theory of finite deformations (see for instance[13]) one can express the rate of material strains as $\dot{\mathring{a}}_{mat} = \mathbf{F}^{T} \cdot \mathbf{d} \cdot \mathbf{F}$, where $\mathbf{F}$ = displacement gradient, with Cartesian components $F_{ij} = \partial x_i / \partial X_j$, and $\mathbf{d}$ = rate of deformation, with Cartesian components $d_{ij} = (\partial \dot{u}_i / \partial x_j + \partial \dot{u}_j / \partial x_i)/2$. In this case, we can approximate $\mathbf{F} \cong \mathbf{R}$, rotation of this point at the time of interest, and for very small time increments Δt one can also write $\dot{\mathring{a}}_{mat} = \ddot{A}\mathring{a}_{mat}/\Delta t$, and $\dot{u}_i = \Delta u_i / \Delta t$, which leads to:

$$\Delta \mathring{a}_{mat} = \mathbf{R}^{T} \cdot \Delta \mathring{a} \cdot \mathbf{R} \tag{1}$$

where $\ddot{A}\mathring{a}$ is the symmetric gradient of the (small) increments of displacements, with Cartesian components:

$$\ddot{A}\mathring{a}_{ij} = \frac{1}{2}\left(\frac{\partial \Delta u_i}{\partial x_j} + \frac{\partial \Delta u_j}{\partial x_i} \right) \tag{2}$$

Note that this definition is analogous to that of standard small strain theory, and therefore $\ddot{A}\mathring{a}$ also corresponds to the strain increment calculated with a standard small strain FE program, in which the nodal coordinates have been updated to their current locations by summing displacements to the initial coordinates.

Once material strain increments have been obtained, using the constitutive law one may obtain material stresses, these may be then converted to spatial stresses using the push-forward operation, which in this case may be approximated as the rotation:

$$\acute{o}_{spa} = \mathbf{R}^{T} \cdot \acute{o}_{mat} \cdot \mathbf{R} \quad ; \quad \acute{o}_{mat} = f(initial\ state, \ddot{A}\mathring{a}_{mat}) \tag{3}$$

Analogous concepts and relations may be developed also for the interface relative displacements and tractions.

Having total spatial stresses at each point of the continuum and interface elements, equivalent nodal force contributions for each element are obtained with the traditional small strain integral expression $\mathbf{f}_{el} = \int \mathbf{B}^\mathbf{T} \hat{\sigma} \, dV$, which also holds if matrix $\mathbf{B}$ has been calculated with the updated coordinates. These total nodal forces are then compared to the external applied loads and, new residuals are obtained for the next iteration.

5 NUMERICAL RESULTS IN TENSION

The first results presented correspond to uniaxial tension, applied on the meshes with solid boundaries (Figure 2 up). The load is applied along the *y*-axis. Uniform displacements are prescribed to all nodes of the upper and lower specimen edges, while transverse displacements are left free. Average stresses are obtained by summing nodal reactions and dividing by specimen size. Constitutive parameters are given by the following values: $E = 900$MPa, $\nu = 0.18$, and for the interface $K_N = K_T = 10^9$MPa/m, tensile strength $\chi_0 = 32$MPa, $c_0 = 100$MPa, $\tan\phi = 0.8$, $G^I_f = 2.2$N/mm, $G^{IIa}_f = 10G^I_f$, $\sigma^{dil} = 10$ MPa (all other parameters equal to zero). Note that elastic stiffnesses K_N, K_T for interfaces are assigned very high values compatible with not causing numerical difficulties. The iterative strategy used is an arc length-type procedure, in order to obtain convergence near and after the peak load[6]. The numerical results obtained with and without the nonlinear geometric effects are represented in Figure 4 together with experimental curve.
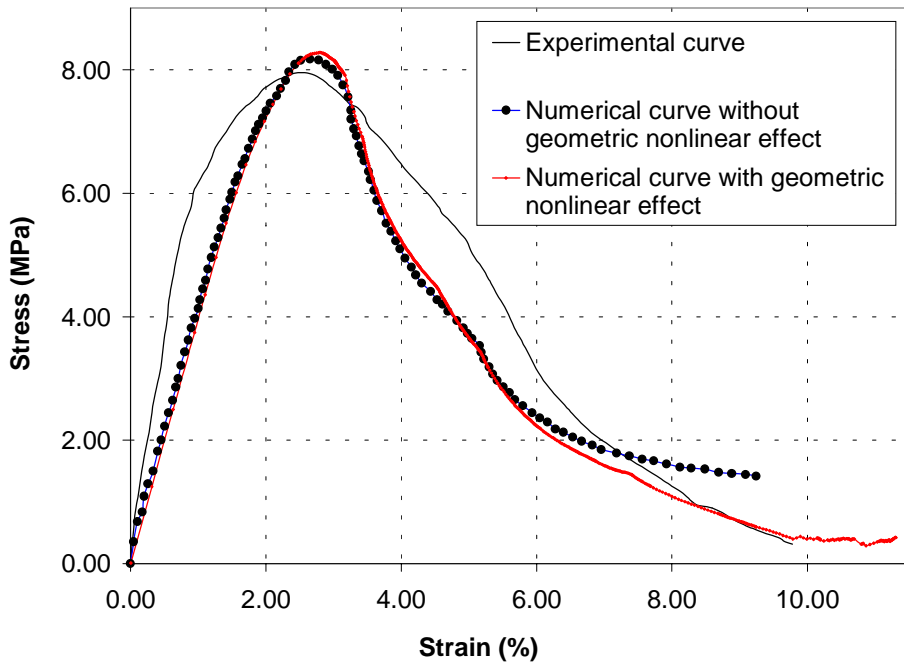
Figure 4. Average stress-strain curves in uniaxial tension.

In Figure 5, the situation at the end of the curve with geometrically non-linear effects, is depicted in some detail. Figure 5a shows the fracture energy spent (W^{cr}) at every interface integration point. In Figure 5b, the deformed mesh at that same stage is represented.
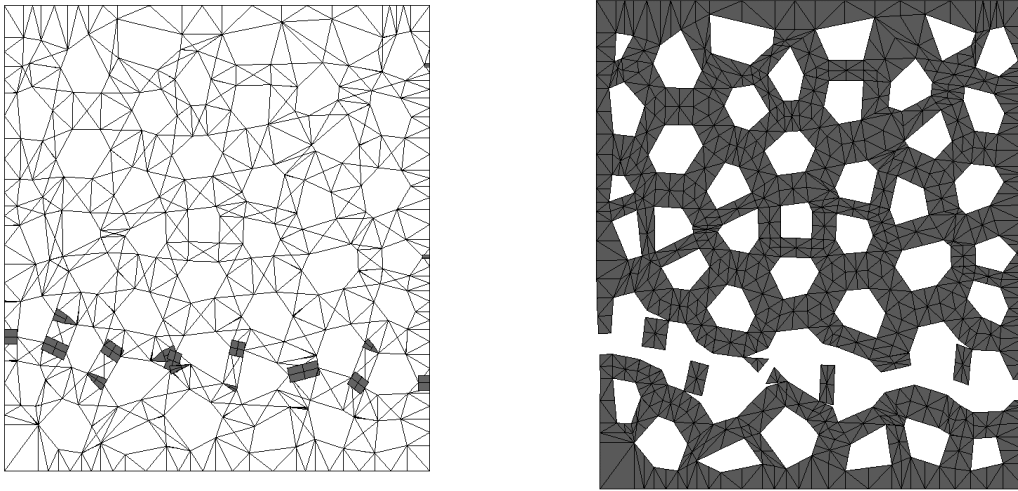
Figure 5. Final state in uniaxial tension with non-linear geometric effects, in terms of energy spent at interfaces (left) and deformed mesh (right). Magnification factor = 2.

The failure pattern observed is as expected approximately horizontal, which agrees with commonly observed crack patterns in tension.

One clear consequence of including non-linear geometric effects in the analysis is that the resulting average stress-strain curve really decreases to zero for large prescribed tensile strain, (similar to what the experimental curves show), while without those effects it tends to an unrealistic horizontal plateau with apparent "residual friction" (Figure 4). This is due to the bridges of material between the two separating sides, which in linear geometric analysis are implicitly assumed to remain with their original orientation, while in reality they may be experiencing significant rotations. Shear and normal stresses on the interfaces may therefore be not captured adequately.

6 NUMERICAL RESULTS IN COMPRESSION

Figures 6 and 7 depict the results obtained with the mesh without solid boundary (Figure 2 down), subjected to uniaxial compression along vertical axis y. The parameter values used are: $E = 2600$MPa, $\nu = 0.2$, and for the interface $K_N = K_T = 10^9$MPa/m, tensile strength $\chi_0 = 10$MPa, $c_0 = 60$MPa, $\tan\phi = 0.6$, $G^I_f = 0.5$N/mm, $G^{IIa}_f = 10G^I_f$, $\sigma^{dil} = 10$ MPa, $\alpha^{dil}_\sigma = -3$, and all other parameters equal to zero. In Figure 6, the macroscopic average stress-strain curves, with and without considering non-linear geometric effects, are represented together with experimental results[14]. The curve for large displacement formulation is stopped at the point reached by the on-going calculations at the time of delivering this paper.
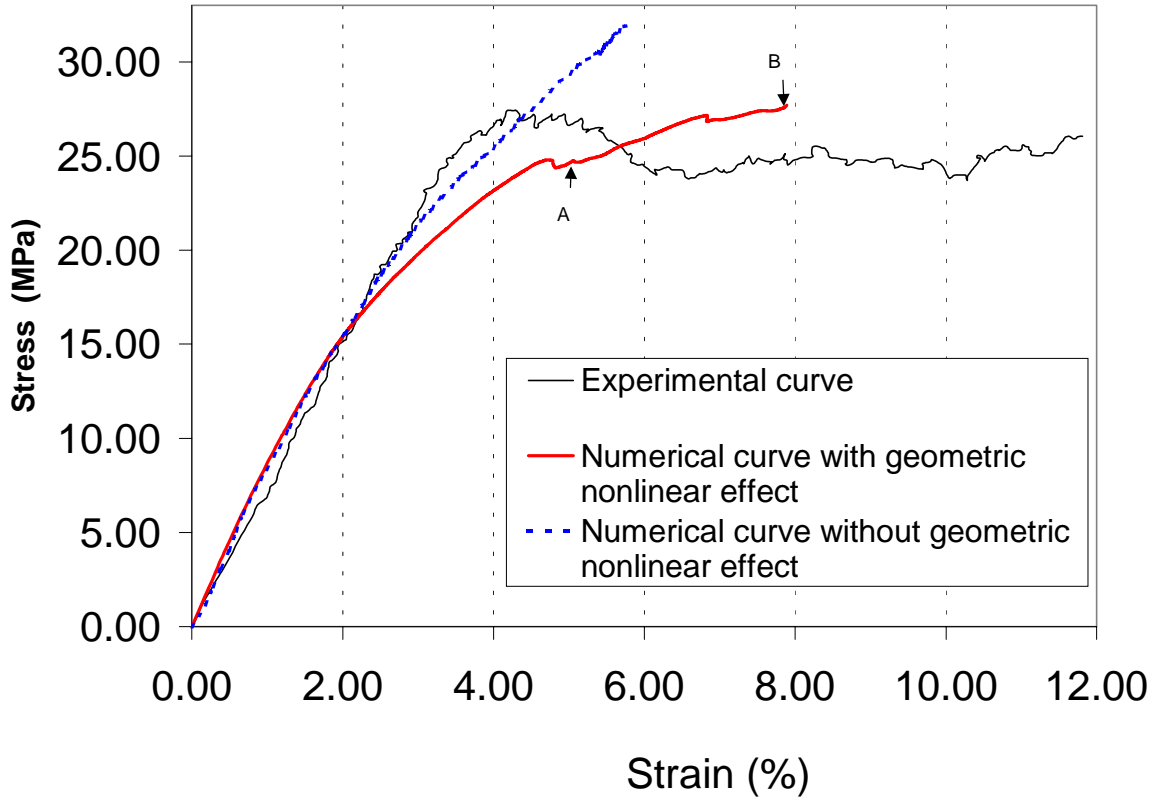
Figure 6. Average stress-strain curves in uniaxial compression.

Figure 6, clearly shows that not considering large displacements may lead to unrealistically high compression peak loads (or no peak at all in some cases), even if nonlinear material laws with softening are considered. The curve calculated with non-linear geometric effects looks much more realistic, if compared with the experimental one, with a clear tendency to a horizontal plateau.

Figure 7 depicts the details of an intermediate and advanced states of uniaxial compression (points A and B in previous curve), in terms of the fracture energy spent in interfaces (left) and deformed mesh (right). In the latter, a clear pattern of void crushing may be observed. However, careful examination of both pictures shows a new limitation. Mesh overlaps are clearly appearing in a few areas marked by circles, which correspond to the interfaces with the largest shear relative displacements (since G^{IIa}_f is much higher than G^I_f, energy spent in shear quickly overtakes the energy that can be spent in tension). This would be physically unacceptable, and therefore to proceed further with the compressive loading, we may need to address the problem of new contacts forming between initially unrelated elements around the

8

perimeter of each void. This remains the next challenge to take up in the ongoing study.
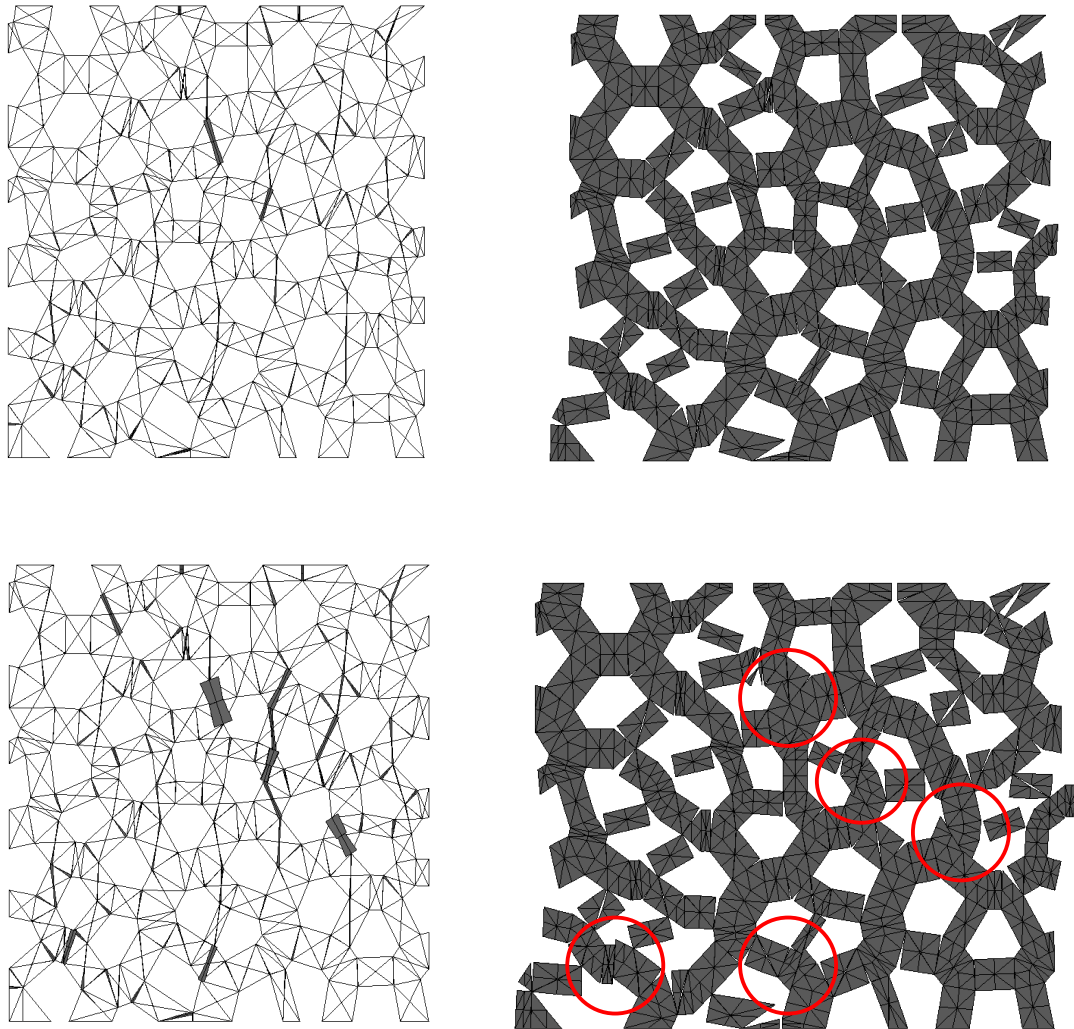
Figure 7. Intermediate (up) and final state (down) in uniaxial compression with non-linear geometric effects, in terms of energy spent at interfaces (left) and deformed mesh (right). Magnification factor = 1.5.

7 CONCLUDING REMARKS

A micromodel initially developed and successfully verified for concrete analysis, is now being applied to cancellous bone. For this application, the model has required further development in order to include the effects of large nodal displacement (while strains in the continuum and relative displacements in interfaces are assumed to remain small). The results obtained seem reasonable and fit qualitatively well the experimental curves in tension, where

spurious residual stresses which were observed with the geometrically linear analysis, can be successfully eliminated. In compression, the large displacement formulation implemented also allows us to proceed further in the analysis, with a clear tendency to a horizontal plateau. This considerably improves the always-increasing response of the geometrically linear theory. However, in this loading case we reach a new limitation when mesh overlaps start to appear at the ends of highly sheared interface elements.

ACKNOWLEDGEMENTS

REFERENCES

[1] S.C. Cowin, "The relationship between the elasticity tensor and the fabric tensor." *Mech. Mater*, A-137-147 (1985).

[2] R.Huiskes, "Adaptative bone-remodeling theory applied to prosthetic design-analysis." *J. Biomechanics*, **20**:1135-1150 (1987).

[3] C.H, Turner, S.C. Cowin, R.B. Ashman, and J.C. Rice, "The Fabric Dependence of Orthotropic Elastic Constants of Cancellous Bone." *J. Biomechanics* **23**:549-561 (1990).

[4] T. Stankowski, *Numerical simulation of progressive failure in particle composites*. PhD thesis, Dept. CEAE, University of Colorado, Boulder, CO 80309-0428, USA (1990).

[5] R. Vonk, *Softening of concrete loaded in compression.* Doctoral Thesis, Technische Universiteit Eindhoven, Postbus 513, 5600 MB Eindhoven, Netherlands (1992).

[6] C.M. López, *Microstructural analysis of concrete fracture using interface elements. Application to various concretes* (In Spanish). Doctoral Thesis. Universitat Politecnica de Catalunya. ETSECCCP-UPC, E-08034 Barcelona, Spain (1999).

[7] R. Huiskes, and S.J. Hollister, "From structure to process organ to cell: recent developments of FE-analysis in orthopaedic biomechanics". *Transactions of the ASME*, **115**:520-527 (1993).

[8] P.J. Prendergast, "Prediction of Bone Adaptation using damage accumulation." *J. Biomechanics*, **27**: 1067-1076 (1994).

[9] B. van Rietbergen, H. Weinans, R. Huiskes, and A. Odgaard, "A new method to determine trabecular bone elastic properties and loading using micromechanical Finite-Element method". *J. Biomechanics*, **28**(1):69-81 (1995).

[10] M. Pini, C.M. López, I. Carol and R. Contro, "Microstructural analysis of cancellous bone using interface elements." In H.P. Rossmanith Editor, *Damage and Fracture of Interfaces (DFI-1),* Balkema, pp. 431-437 (1997).

[11] I. Carol, P.C. Prat, C.M. López, "A normal/shear cracking model. Application to discrete

crack analysis". *J. of Engineering Mechanics*. Vol. **123**, No 8 (1997).

[12] I. Carol, P.C. Prat, "A multicrack model based on the theory of multisurface plasticity and two fracture energies". In Owen, D.R.J., Oñate, E., and Hinton, E., editors, *Computational plasticity 4*, Pineridge Press (Swansea, UK), pp.1583-1594, (1995).

[13] L. Malvern, Introduction to the mechanics of a continuum medium. Prentice-Hall (1969).

[14] P. Pisoni, Confronto tra risultati numerici e risultati sperimentali della risposta tensionale di un campione di osso spongioso. Tesi di Laurea. Politecnico di Milano. Italy. (1998).